



TOMOGRAPHIC RECONSTRUCTION OF THE MOMENTS OF LOCAL PROBABILITY DENSITY FUNCTIONS IN TURBULENT FLOW FIELDS

MARC R. NYDEN,^{a*} PUMYOS VALLIKUL,^{a,†} and Y. R. SIVATHANU^{b,‡}

^aBuilding and Fire Research Laboratory, National Institute of Standards and Technology, Gaithersburg, MD 20899 and ^bSchool of Mechanical Engineering, Purdue University, West Lafayette, IN 47907-1003, U.S.A.

(Received 25 April 1995)

Abstract—An algorithm for the tomographic reconstruction of the individual moments of the probability density functions describing the local transmittance of radiation through a turbulent flow field is advanced. The new method, which is based on Fourier inversion, is applicable to asymmetric (as well as, to axisymmetric) flows. The validity of the method is examined by comparing reconstructed moments of the local probability functions in a buoyant propene/air flame and an ethene/air jet flame to the corresponding values obtained from optical probe measurements.

INTRODUCTION

The chemical processes which determine combustion efficiency are distributed throughout the reacting volume. The existing methods for continuous process monitoring in combusting flows, however, are based on sampling the composition at a few representative points in the reactor (e.g., with thermocouples) and/or on path integrated concentrations obtained from line-of-sight measurements through the exhaust stream (e.g., with open path FTIR). The information obtained in either case is poorly resolved in both space and time and has limited diagnostic value. A further deficiency of the point-sampling approach is that the measurement probes are inserted directly into the reactor where they are subjected to extreme temperatures and corrosive byproducts which adversely affect their performance and reliability. These problems can be circumvented by using computed tomography to reconstruct the local transmittance [$\tau_v(x, y)$] and emission of radiation at specific frequencies (ν) from a series of line-of-sight measurements, $\tau_{is\nu}(r, \theta)$.

Tomographic spectroscopy has been applied in numerous previous investigations of laminar flames and other steady-state phenomena.^{1–5} The focus of this paper is on the application of tomography to the study of turbulent flow systems, which exhibit intermittent composition and temperature. An algorithm for the reconstruction of the local probability density functions (PDFs) which describe the transmission of radiation through a turbulent flow field was advanced in a recent paper by Sivathanu and Gore.⁶ The algebraic reconstruction technique developed by these authors involves a back substitution step, often called “onion-peeling”, which is only valid for axisymmetric flow fields. In the present paper, an alternative approach, which involves the moment-by-moment reconstruction of the local PDFs, is developed and tested. The new method, which is based on a Fourier inversion technique, as opposed to “onion-peeling” is applicable to asymmetric flow fields and is expected to be less sensitive to random errors due to uncertainties in the measurements.^{7–12}

*To whom all correspondences should be addressed.

†Guest Researcher from the Department of Civil, Mechanical and Environmental Engineering, The George Washington University, Washington, DC 20052, U.S.A.

‡Work done at NIST on a Senior Research Fellowship sponsored by ASA/NSF/NIST.

THEORY

Radiation field

The spectral distribution of the radiant energy in a combusting flow field is a function of the temperature of the source (emission) and the composition of the medium (transmission). In principle, this means that the reaction conditions in any volume element (voxel) of the reactor can be determined from analyses of the spectra corresponding to the emission and transmission of infrared radiation in that region of space.

The flux of radiation from a source voxel which is uniform in temperature (T) is given by

$$R_v(T) = (1 - \tau_v)I_v^b(T). \quad (1)$$

In this equation, $I_v^b(T)$ denotes the blackbody distribution at the temperature, T ,

$$\tau_v = \frac{I_v}{I_{0v}} = \exp(-A_v), \quad (2)$$

is the transmittance, and A_v is the optical depth of the voxel at the frequency, ν . The transmittance can be measured independently from the radiance as the fraction of incident radiation from an external source, I_{0v} , which is transmitted through the voxel (I_v). The radiance measured over a line-of-sight is reduced by absorption of the medium in accordance with Eq. (3).

$$R_v^m(T) = \int R_v[T(x)] \exp\left[-\sum_i A_v(x'_i)\right] dx, \quad (3)$$

where the summation over i includes all voxels along the line-of-sight extending from the source at x to the detector.

In principle, the local concentrations of CO, CO₂, and unburnt hydrocarbon can be determined directly from reconstructions of the absorbance, A_v , at characteristic frequencies. Likewise, the magnitude of the continuum absorption in the reconstructions can be used to estimate the soot volume fraction. The local temperature can be determined by fitting the ratios of the reconstructed radiance and absorbance spectra, $R_v/(1 - \tau_v)$, to the theoretical blackbody distribution, $I_v^b(T)$.

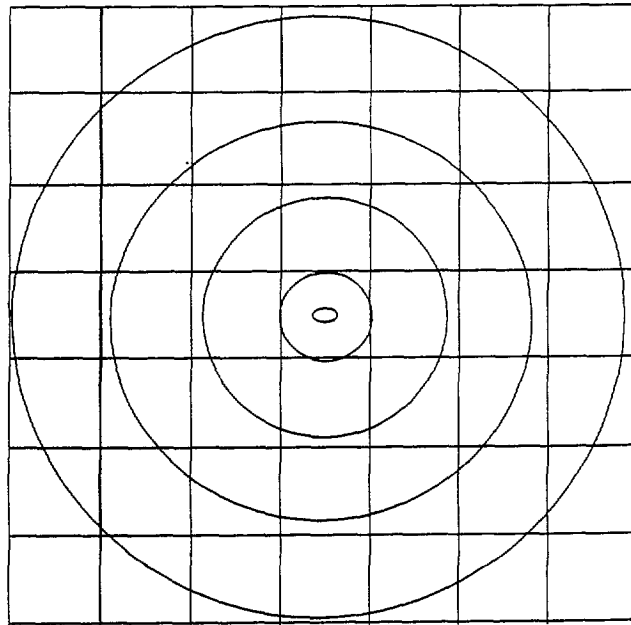


Fig. 1. The PDFs of an axisymmetric flow field superimposed on a Cartesian grid. The rings represent regions of constant PDF. The separation between voxels is on the order of the integral scale of the turbulence.

Model of an axisymmetric turbulent flow field

The PDF structure corresponding to an axisymmetric flow field is depicted in Fig. 1. The reconstruction algorithm, which is the focus of this paper, is based on the assumption that the local transmittance of radiation through a voxel can be described by a set of stochastically independent random variables. A necessary (but not sufficient) condition for the validity of this assumption is that the separation between voxels (depicted as a Cartesian grid) must be on the order of the integral scale (L_E) of the turbulent flow. To the extent that this is a valid assumption, the joint PDF of the transmittance (at any frequency) through a line-of-sight spanning n voxels is given by a simple product of the local PDFs as represented in Eq. (4).¹³

$$P(\tau_1, \tau_2, \dots, \tau_n) = P_1(\tau_1)P_2(\tau_2) \dots P_n(\tau_n). \quad (4)$$

Consequently, the expected value of any moment ($m = 1, 2, \dots$) of the line-of-sight transmittance ($\tau_{ls} = \tau_1 \tau_2 \dots \tau_n$) is

$$\begin{aligned} \int P(\tau_{ls}) \tau_{ls}^m d\tau &= \int \dots \int P(\tau_1) \dots P(\tau_n) \tau_1^m \tau_2^m \dots \tau_n^m d\tau_1 d\tau_2 \dots d\tau_n \\ &= \langle \tau_1^m \rangle \langle \tau_2^m \rangle \dots \langle \tau_n^m \rangle, \end{aligned} \quad (5)$$

where the quantities in angular brackets are the expected values of the moments of the local transmittance in each voxel.

The conventional algorithms for tomographic reconstruction are based on a linear relationship between the image [right-hand side of Eq. (5)] and its projection (left-hand side). In this case, linearization is easily accomplished by taking the (negative) logarithm of both sides of the equation. The result, expressed in Eq. (6), provides a measure of the average optical depth and is the foundation for the moment-by-moment reconstruction of the local PDFs in a turbulent flow field.

$$-\ln \langle \tau_{ls}^m \rangle = \sum_{i=1}^n -\ln \langle \tau_i^m \rangle. \quad (6)$$

Fourier reconstruction of local PDFs

The basis of Fourier inversion is the so called "central slice" theorem which states that the one-dimensional Fourier transform of the line-of-sight projection taken from a view specified by the angle θ , is a slice through the two dimensional Fourier transform of the local property field.⁷⁻¹² Application of the convolution theorem gives the moments of the local PDFs as the filtered back projection,

$$-\ln \langle \tau(x, y)^m \rangle = \frac{1}{2\pi} \int d\theta \int [-\ln \langle \tau_{ls}(r, \theta)^m \rangle \phi((x \cos \theta + y \sin \theta) - r)] dr, \quad (7)$$

of the line-of-sight moments, measured at regular intervals (Δr) along an axis of each of a series of view angles. The filter function, $\phi(r)$, is the (approximate) inverse Fourier transform (of the absolute value) of the spatial frequency variable $|\omega|$ which is complementary to r (axial distance).

The assumption of stochastic independence limits the spatial resolution of the measurements to L_E . Any further subdivision of the measurement space will introduce errors due to spatial correlation. This is an unfortunate limitation, since it implies that it may not always be possible to eliminate sampling errors in the reconstruction without introducing correlation errors.

EXPERIMENTAL

The moment-by-moment algorithm was tested on the same data set used in the validation of the Sivathanu-Gore method.^{6,14} The reconstructed moments of the local transmittance of radiation at 632.8 nm (from a HeNe laser) are compared to the corresponding moments computed from measurements obtained using a purged optical probe sampling over a 0.01 m path. The optical depth at this frequency is proportional to the soot volume fraction. Independent measurements were made at $x/d = 6.7$ in a propene/air flame (50 mm dia at the base) which had an exit Reynolds number of 670¹⁴ and at $x/d = 30$ in an ethene/air jet flame (6 mm dia) with an exit Reynolds number of 9200.⁶ Each PDF summarizes the results obtained from 10⁵ measurements of the transmission

of the laser through the flame in increments of 0.01 transmittance units. The uncertainty in the measurements was estimated from the standard deviation of the transmittance (with respect an average value of 1.000) over a short path (~ 1 m) through the atmosphere in the absence of the flame. The value obtained in this way was 0.8%.

Measurements were made at 11 positions, both within (probe) and through (line-of-sight) the ethene/air flame, which were spaced at intervals of 0.005 m extending from the centerline to the edge of the luminous region. Line-of-sight data were not available in the case of the propene/air flame. Instead, the path integrated PDFs were synthesized as the product of the local PDFs¹⁵ obtained from optical probe measurements made at 12 interior positions from the centerline to the edge of the luminous region which were spaced 0.007 m apart. The use of synthetic line-of-sight data permits a direct evaluation of the inversion algorithm independent of the errors due to spatial correlation.

The Fourier reconstructions of the moments were performed in accordance with Eq. (7) with the filter function described in Ref. 12. The integrals were evaluated by quadrature using 100 view angles. In the applications involving axisymmetric flow fields, the same projection, τ_{ls} , was used for every view. In the example used to demonstrate the applicability of the algorithm to asymmetric flow fields, the projections were obtained by rotating the function $\tau_{ls}(x, y)$ by the corresponding view angle.

RESULTS AND DISCUSSION

Propene/air flame

The validity of Eq. (6) was tested by comparing the moments of the transmittance, as computed by integrating the moments of the probe measurements over the line-of-sight (right-hand side), to the corresponding values obtained from the line-of-sight PDFs (left-hand side). In the case of the propene/air flame the left-hand side was actually computed from the synthetic line-of-sight PDFs which were constructed point-by-point in accordance with the algorithm described in Ref. 15. The values of the transmittance obtained from optical probe measurements were renormalized to the appropriate path length in accordance with Eq. (8).

$$\langle \tau_l \rangle = \langle \tau_p \rangle^{l/0.01}, \quad (8)$$

where τ_l denotes the transmittance over a distance of l m in a region of constant PDF and τ_p is the transmittance measured over the separation of the optical probes (0.01 m) in a region of the flame having the same PDF. This equation is an obvious corollary of Eq. (5) which applies to stochastically independent regions described by the same PDF.

The first and second moments of the line-of-sight PDFs (points) and the corresponding values obtained by integrating the moments of the probe PDFs over the line-of-sight (solid curve) are depicted in Figs. 2 and 3. The same excellent agreement was observed for the higher moments, as well, thereby corroborating the validity of Eq. (6) for the description of the local PDF structure of turbulent flames.

The reconstructed first and second moments (normalized to a path length of 0.01 m), as computed from Eq. (7), are compared to the actual probe measurements (points) in Figs. 4 and 5. The agreement is comparable in the higher moments which, once again, are not displayed in the interest of brevity. The step-like behavior of the probe data is a consequence of the assumption that the local PDFs are constant over the sampling interval (0.007 m). The low sampling frequency of the line-of-sight measurements introduces an aliasing error in the reconstruction of the measured data (solid line) which is not apparent in the reconstructions computed from the probe moments (dashed line) where the integration in Eq. (7) is performed over a much finer numerical grid.

It is of interest to note that the curve which describes the variation of the second moments as a function of axial distance is almost identical to the curve obtained by multiplying the first moment by two. This is an obvious consequence of the sharpness of the PDFs. Indeed, Eq. (9)

$$\langle \tau^m \rangle - \langle \tau \rangle^m, \quad (9)$$

is exact for a δ -function PDF; which is the case in a laminar flow field. In a turbulent flame, the sharpness of the PDF is measured by the magnitude of the deviations from the mean [i.e.,

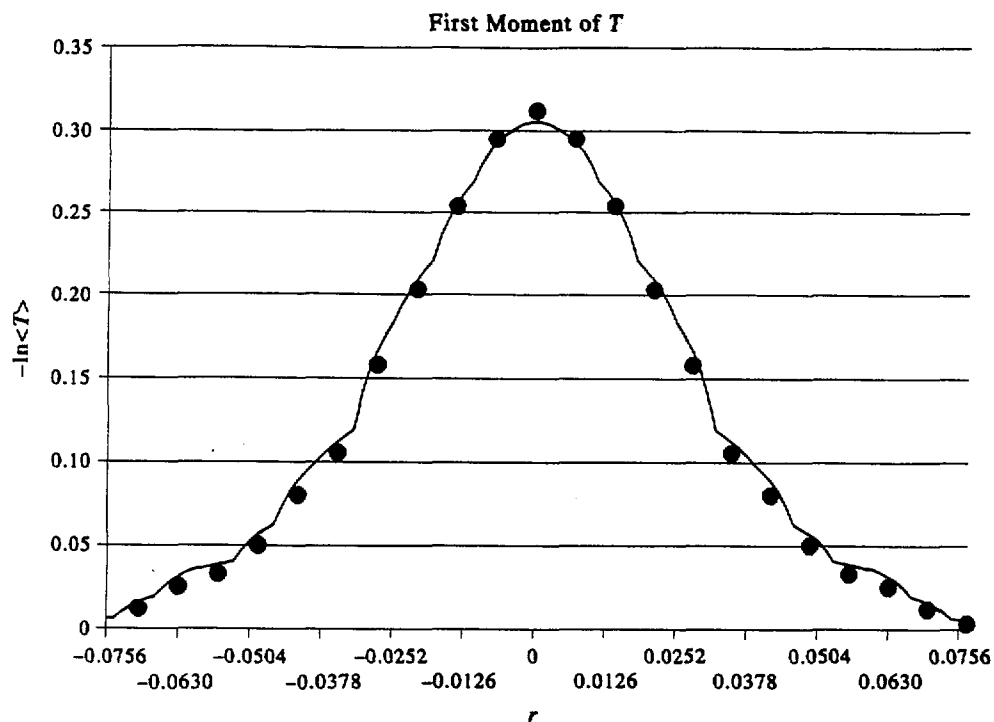


Fig. 2. The negative logarithm of the first moment of the line-of-sight transmission measurements (points) and the values computed by integrating the moments of the probe measurements over the corresponding line-of-sight in the propene/air flame (solid line).

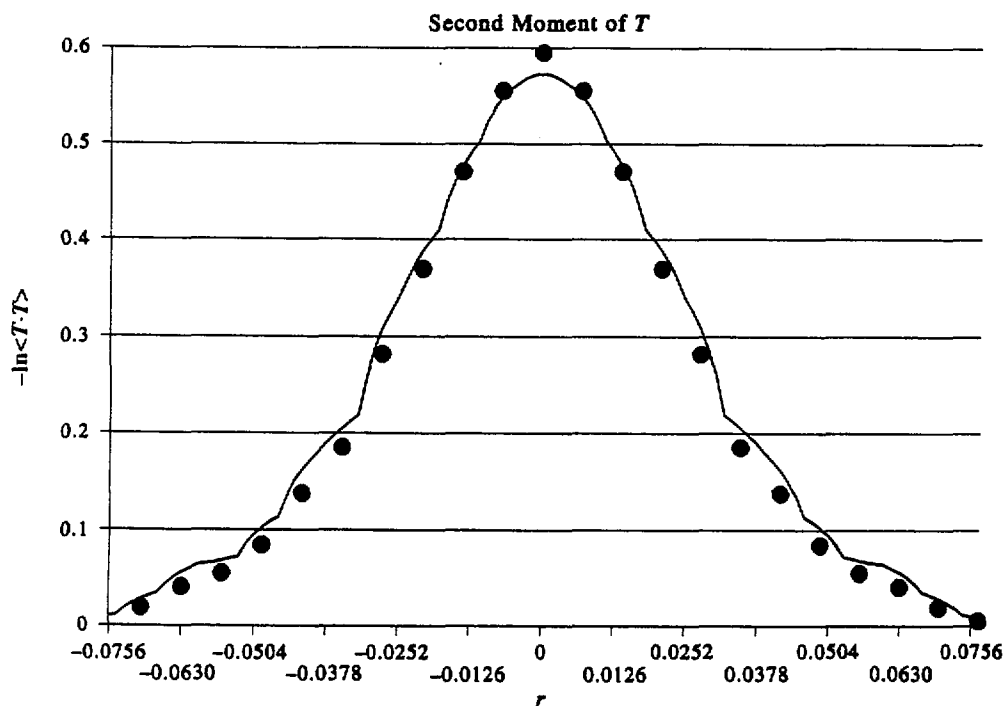


Fig. 3. The negative logarithm of the second moment of the line-of-sight transmission measurements (points) and the values computed by integrating the moments of the probe measurements over the corresponding line-of-sight in the propene/air flame (solid line).

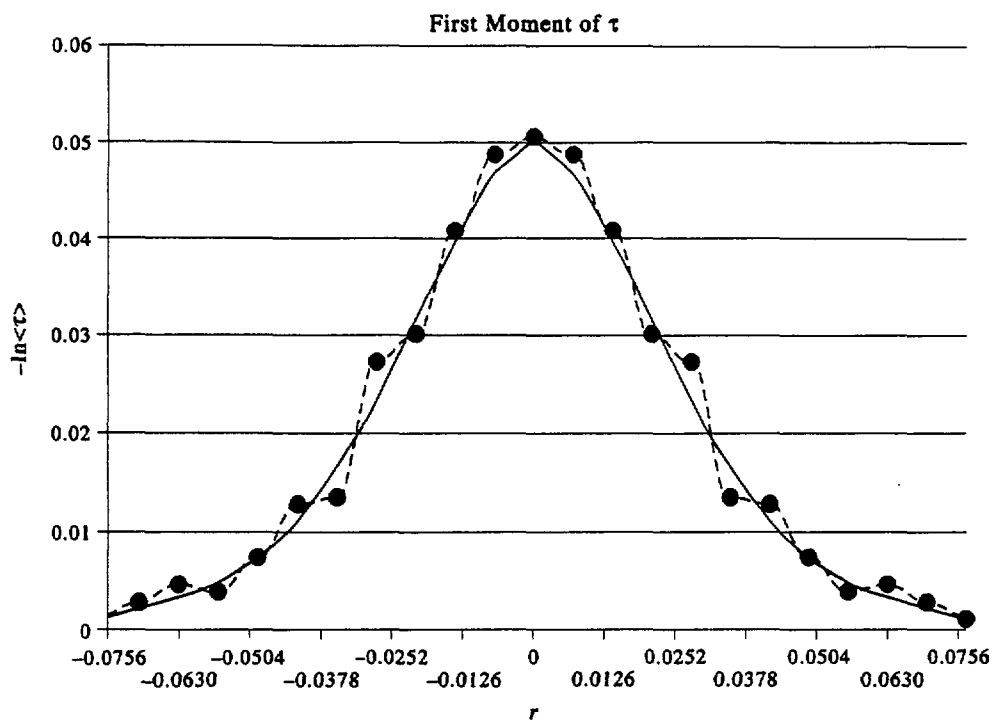


Fig. 4. The negative logarithm of the first moment of the local PDFs reconstructed from the line-of-sight measurements (solid line) and from the integral of the moments of the probe measurements over the corresponding line-of-sight (dashed line) are compared to the measured values from the propene/air flame (points).

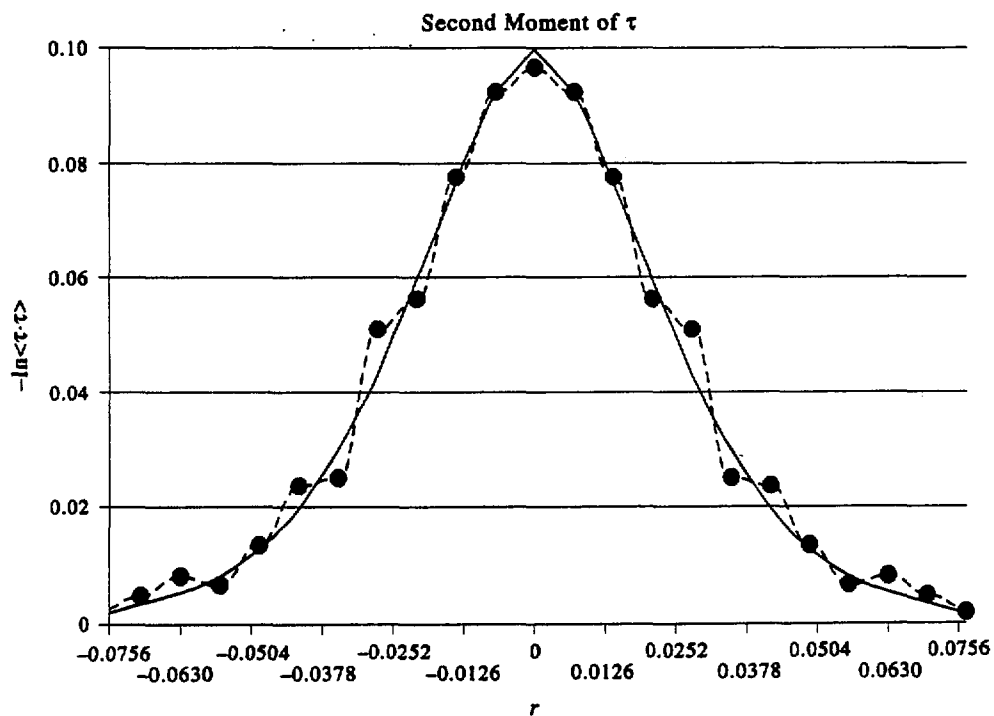


Fig. 5. The negative logarithm of the second moment of the local PDFs reconstructed from the line-of-sight measurements (solid line) and from the integral of the moments of the probe measurements over the corresponding line-of-sight (dashed line) are compared to the measured values from the propene/air flame (points).

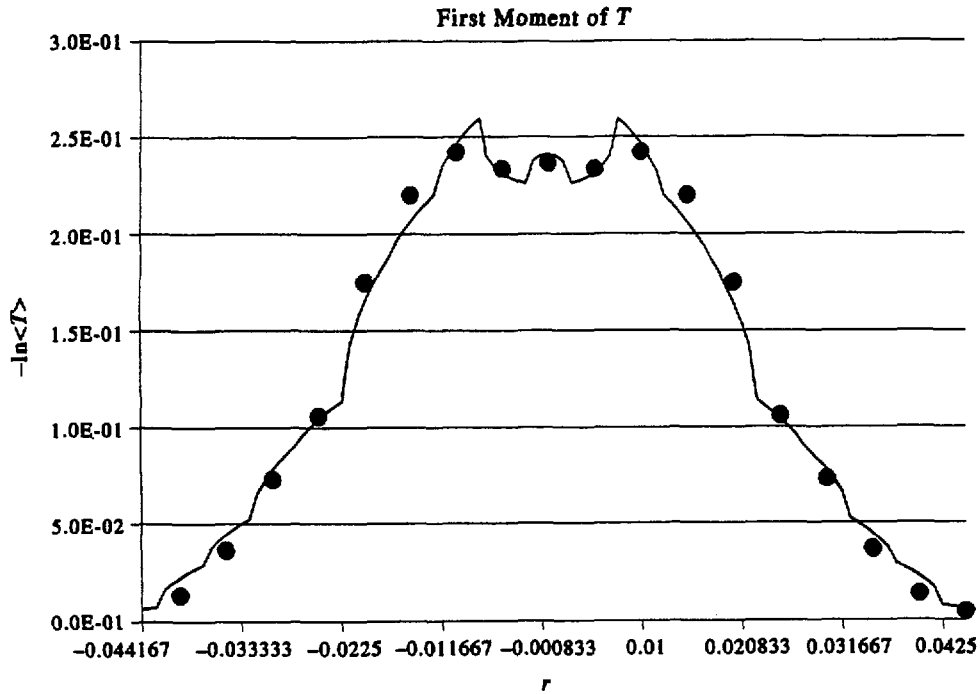


Fig. 6. The negative logarithm of the first moment of the line-of-sight transmission measurements (points) and the values computed by integrating the moments of the probe measurements over the corresponding line-of-sight in the ethene/air flame (solid line).

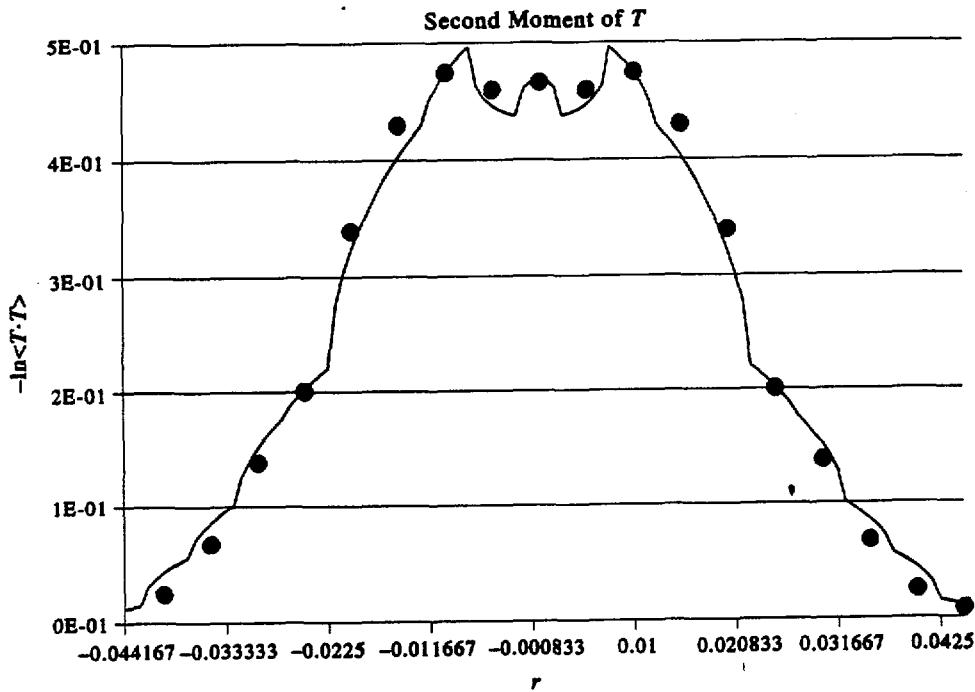


Fig. 7. The negative logarithm of the second moment of the line-of-sight transmission measurements (points) and the values computed by integrating the moments of the probe measurements over the corresponding line-of-sight in the ethene/air flame (solid line).

$\{\langle(\tau - \langle\tau\rangle)^m\rangle\}^{1/2}$. This quantity will become negligibly small at some value of m which determines the number of moments required to characterize the turbulent flow field. In the case of the propene/air flame, the turbulent intensity at $m = 2$ is already less than 10% of the mean transmittance at every axial distance.

Ethene/air flame

The path integrated values of the negative logarithms of the first and second moments of the probe measurements (solid lines) are compared to the corresponding moments of the line-of-sight PDFs (points) in Figs. 6 and 7. The excellent agreement between the left- and right-hand sides of Eq. (6) indicates that the spatial correlation errors are negligible with respect to the magnitude of the moments. The path integrated values were computed by summing the local moments from the probe measurements over each region of constant PDF [Eq. (8)] along the line-of-sight. The optical path length (l) through each region is well defined once the diameter of the flame is determined. Unfortunately, Sivathanu et al did provide a value for this quantity which can be measured directly as (twice) the distance from the centerline to the point where the absorbance falls to zero (within the limits of the experimental error). The diameter of the ethene/air flame (at $x/d = 30$) which was obtained by requiring equality between the first moments of the line-of-sight and path integrated probe measurements at the centerline was 0.087 m. The alternative, would be to assume that $l = \Delta r = 0.005$ m, which is consistent with a diameter of 0.10 m. The former estimate resulted in better agreement between the path integrated and line-of-sight projections. This value is reflected in the path integrated moments plotted in Figs. 6 and 7 and in the renormalization (to correspond to an optical path of 0.01 m) of the reconstructed moments displayed as solid lines in Figs. 8 and 9.

The first two moments obtained from reconstructions of the line-of-sight measurements (solid lines) are compared to the corresponding probe values (points) in Figs. 8 and 9. The largest discrepancies between the measured and reconstructed moments are observed for the interior regions of the flame where the probe measurements exhibit unphysical oscillations. Indeed the moments which were reconstructed from the line-of-sight measurements appear to provide a much more realistic profile of the soot volume fraction than do the moments of the local PDFs measured using optical probes. It is interesting to note that oscillatory behavior of the probe measurements is reproduced in the reconstructions computed from the path integrals of the moments of the probe measurements (dashed lines) even though the corresponding projections are almost coincident with the line-of-sight projections at the radial positions where the measurements were made. In the reconstructions involving the path integrated moments, however, the grid used in the radial integrations was not limited by the availability of experimental line-of-sight measurements so that the aliasing errors could be effectively removed. On the basis of these results, it is clear that the strategy of the oversampling does not necessarily lead to a better description of the structure of turbulent flames.

Asymmetric flow fields

The applicability of the algorithm to asymmetric flows was examined on the basis of the quality of the reconstructions obtained from synthetic line-of-sight PDFs. These distributions were synthesized by integrating the product of the axisymmetric PDFs measured in the propene/air flame with the off-center Gaussian function represented in Eq. (10).

$$P(\tau) = \begin{cases} 1, & \tau = 1 - 0.05 \exp\{(x - 0.028)^2 + (y - 0.028)^2/4\}, \\ 0, & \text{otherwise.} \end{cases} \quad (10)$$

The physical picture corresponds to a steady, asymmetric component superimposed on an intermittent, axisymmetric flow field.

The negative logarithm of the first moment reconstructed from the asymmetric line-of-sight PDFs (top) is compared to the actual values (bottom) as a function of Cartesian coordinates in Fig. 10. The corresponding comparison of the second moment is presented in Fig. 11. The overall agreement for both moments is quite good. In particular, the positions of both peaks are faithfully reproduced. The only notable differences are that the Gaussian feature appears broader and less intense in the reconstructions, and the moments of the turbulent PDFs appear smoother than they do in the plots of the spatial distributions of the actual moments.

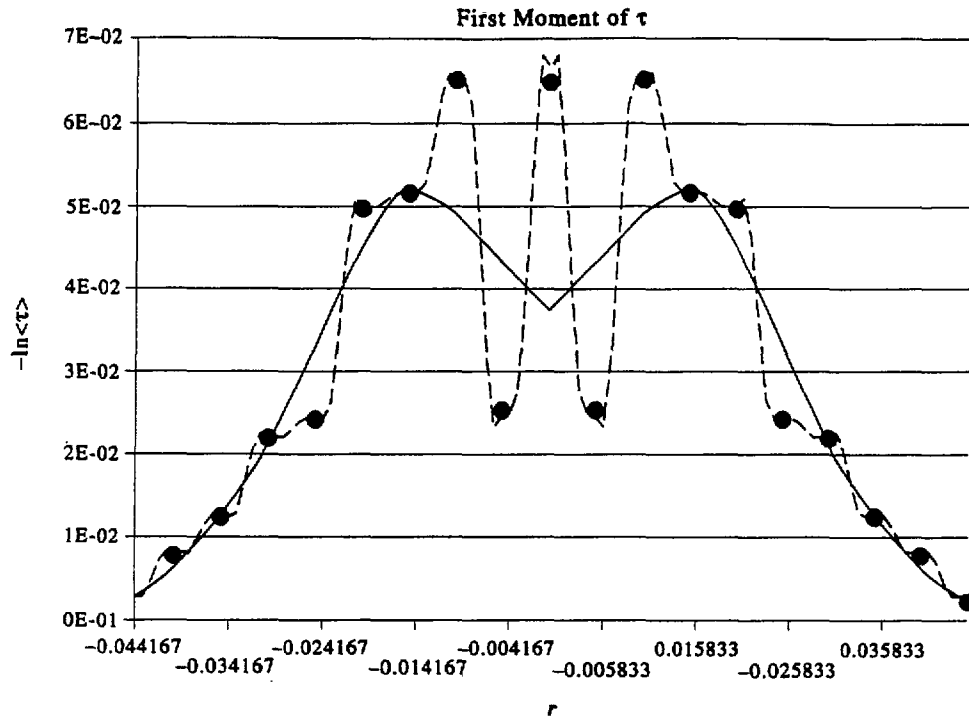


Fig. 8. The negative logarithm of the first moment of the local PDFs reconstructed from the line-of-sight measurements (solid line) and from the integral of the moments of the probe measurements over the corresponding line-of-sight (dashed line) are compared to the measured values from the ethene/air flame (points).

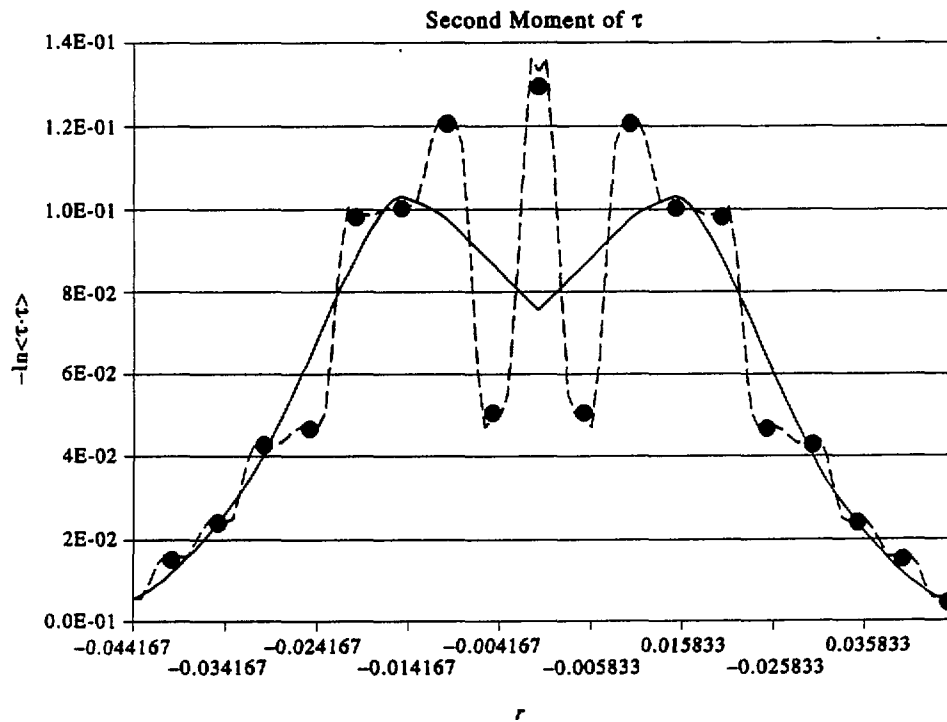


Fig. 9. The negative logarithm of the second moment of the local PDFs reconstructed from the line-of-sight measurements (solid line) and from the integral of the moments of the probe measurements over the corresponding line-of-sight (dashed line) are compared to the measured values from the ethene/air flame (points).

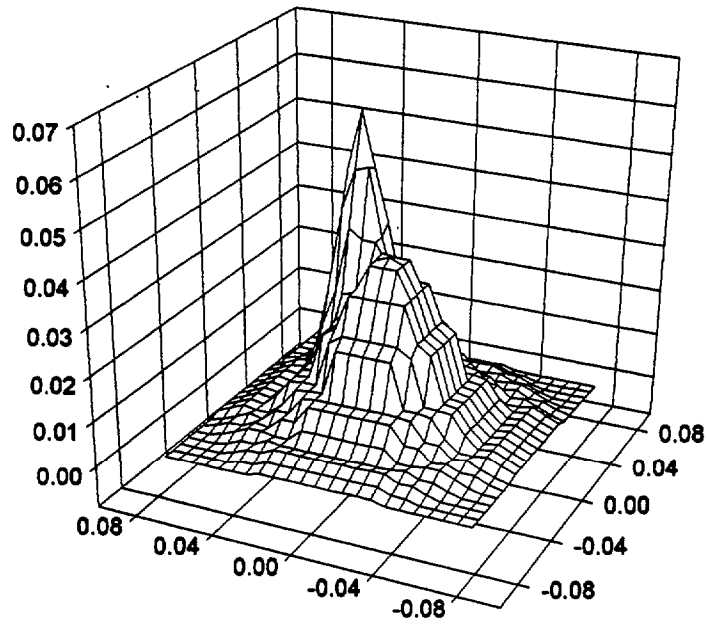
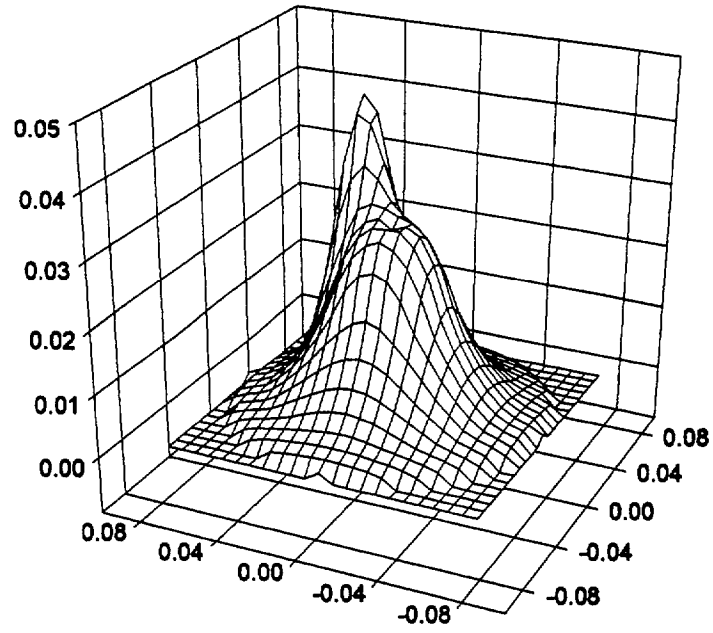


Fig. 10. The negative logarithm of the reconstruction of the first moments of the asymmetric PDFs (top), plotted as a function of (x, y) , are compared to the actual values (bottom).

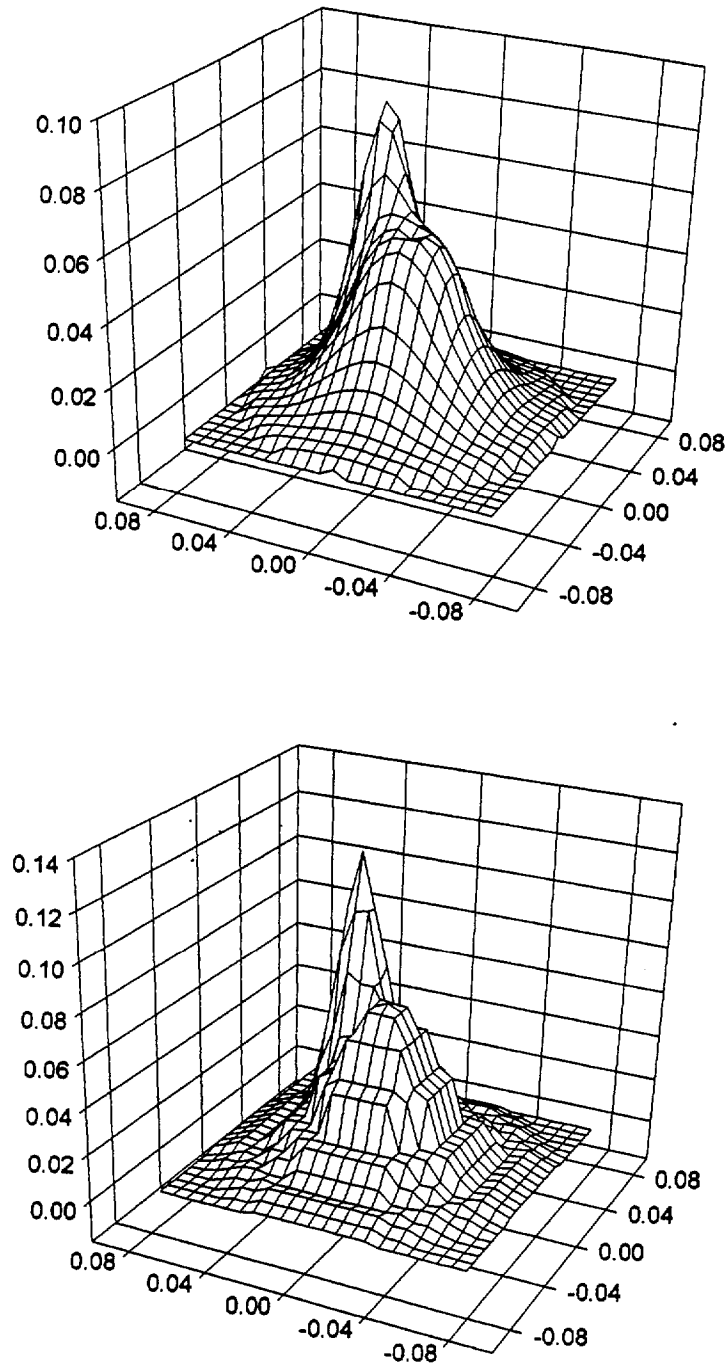


Fig. 11. The negative logarithm of the reconstruction of the second moments of the asymmetric PDFs (top), plotted as a function of (x, y) , are compared to the actual values (bottom).

CONCLUSIONS

An algorithm for the Fourier reconstruction of the individual moments of the local PDFs in a turbulent flow field was developed and tested by comparing the reconstructed moments to measured values obtained from optical probe measurements in two independent flames. This procedure is generally applicable and is a viable alternative to the "onion-peeling" algorithm advanced in a previous paper, which is only valid for axisymmetric flow fields.

In principle, all of the moments are required to determine an arbitrary PDF. In practice, however, the amplitude of the turbulent fluctuations are usually much smaller than the mean transmittance so that expected values of the deviations from the mean tend to fall rapidly to zero. The reconstruction algorithm described in this paper is particularly well-suited to those applications for which a knowledge of the first few moments of the local PDFs are sufficient for an accurate characterization of the flow field.

Acknowledgements—The authors are grateful to Professor Robert Goulard of the George Washington University and to Dr William Grosshandler and Dr Holly Rushmeier of NIST for helpful discussions and good advice.

REFERENCES

1. F. P. Chen and R. Goulard, *JQSRT* **16**, 819 (1976).
2. P. J. Emmerman, R. Goulard, R. J. Santaro, and H. G. Semerjian, *J. Energy* **4**, 70 (1980).
3. R. J. Santaro, H. G. Semerjian, P. J. Emmerman, and R. Goulard, *Int. J. Heat Mass Transfer* **24**, 1139 (1981).
4. P. E. Best, P. L. Chien, R. M. Carangelo, and P. R. Solomon, *Combust. Flam.* **85**, 309 (1991).
5. S. C. Bates, R. Carangelo, K. Knight, and M. Serio, *Rev. Sci. Instrum.* **64**, 1213 (1993).
6. Y. R. Sivathanu and J. P. Gore, *JQSRT* **50**, 483 (1993).
7. S. G. Azevedo, *Model-based Computed Tomography for Nondestructive Evaluation*, Lawrence Livermore National Laboratory (1991).
8. W. Swindell and H. H. Barrett, *Physics Today* **December**, 32 (1977).
9. T. F. Budinger and G. T. Gullberg, *IEEE Trans. Nucl. Sci.* **NS-21**, 2 (1974).
10. Z. H. Cho, *IEEE Trans. Nucl. Sci.* **NS-21**, 44 (1974).
11. G. N. Ramachandran and A. V. Lakshminarayanan, *Proc. natl. Acad. Sci. U.S.* **68**, 2236 (1971).
12. L. A. Shepp and B. F. Logan, *IEEE Trans. Nucl. Sci.* **NS-21**, 21 (1974).
13. A. M. Mood, F. A. Graybill, and D. C. Boes, *Introduction to the Theory of Statistics*, McGraw-Hill, New York, p. 150 (1974).
14. Y. R. Sivathanu and J. P. Gore, *J. Heat Trans.* **114**, 659 (1992).
15. Y. R. Sivathanu and J. P. Gore, *JQSRT* **49**, 269 (1993).